Carnegie Observatories Astrophysics Series, Vol. 2:
Measuring and Modeling the Universe, 2004
ed. W. L. Freedman (Cambridge: Cambridge Univ. Press)

The Polarization of the Cosmic Microwave Background

MATIAS ZALDARRIAGA
Astronomy & Physics Departments, Harvard University

Abstract

We summarize the physical mechanism by which the cosmic microwave background acquires a small degree of polarization. We discuss the imprint left by gravitational waves and the use of polarization as a test of the inflationary paradigm. We discuss some physical processes that affect the cosmic microwave background polarization after recombination, such as gravitational lensing and the reionization of the Universe.

1.1 Introduction

Since its discovery in 1965 the cosmic microwave background (CMB) has been one of the pillars of the Big Bang model (Penzias & Wilson 1965). The various measurements of its spectrum, in particular by the *COBE*/FIRAS instruments firmly established the hot big bang model as the basis of our understanding of cosmology (Mather et al. 1994).

The study of the spectrum was followed by the detection of tiny anisotropies in the CMB temperature, first by *COBE*/DMR (Smoot et al. 1992), and then by a variety of more sensitive experiments with better angular resolution*. The anisotropies, a natural consequence of the structure formation process, contain a wealth of information about the cosmological model. They depend on the matter content of the Universe and on the physical process that created the tiny seeds that grew under gravity to form the structure in the Universe around us. Moreover, the structure formation process leaves its imprint on the CMB through secondary effects such as gravitational lensing, the Sunyaev-Zel'dovich effect (Sunyaev & Zel'dovich 1972), or the Ostriker-Vishniak effect (Ostriker & Vishniak 1986).

The detailed study of the temperature anisotropies has taken the field into the era of "precision cosmology." Ever more sensitive temperature experiments have so far confirmed our theoretical picture. These studies have revealed the presence of acoustic peaks in the power spectrum and of a damping tail on small scales. The comparison of measurements and theory, most recently the results of *WMAP* (Hinshaw et al. 2003), have led to very narrow constraints on several of the cosmological parameters. Experiments already under way or being constructed, such as the *Planck* satellite, will tighten constraints even further. We warn the reader that this article was written prior to the release of the *WMAP* results; references to them were added just before publication.

The next big goal for CMB experimentalists was the detection of the even smaller CMB

* A compilation of up to date results can be found at http://www.hep.upenn.edu/~max/ . We apologize for not giving an up to date list of all experiments but that made us exceed the page limit.

polarization anisotropies. This was accomplished for the first time by the beautiful DASI experiments (Kovac et al. 2002; Leitch at al. 2002). Since the first detection of the CMB, there have been many theoretical studies of the expected polarization properties (e.g., Rees 1968; Polnarev 1985) and numerous attempts to measure or put upper limits on it. Figure 1.1 provides a summary of experimental results up to the time of writing. "Modern" experiments include POLAR (Keating et al. 2001) and PIQUE (Hedman et al. 2002), which set the most stringent upper limits before the DASI detection, roughly around 10 μK. The correlation between temperature and polarization was searched for by comparing PIQUE with Saskatoon (de Oliveira-Costa et al. 2003, 2004), was detected by DASI, and has now been measured with exquisite signal-to-noise ratio over a wide range of scales by *WMAP* (Kogut et al. 2003).

DASI opened a new window into the early Universe. Polarization is sensitive to most of the parameters in the cosmological model. The way it depends on them is often different than the way temperature anisotropies do. As a result, accurate measurements of the CMB polarization will improve the determination of many cosmological parameters (Zaldarriaga, Spergel, & Seljak 1997; Eisenstein, Hu, & Tegmark 1999). Moreover, polarization will provide an excellent test bed for consistency check on parts of the model that at present we take for granted.

The big push toward polarization, however, comes from its potential as a detector of a stochastic background of gravitational waves (GW). It has been shown that the pattern of polarization "vectors" on the sky will be different—it will have a curl-like component—if there is a stochastic background of GW (Kamionkowski, Kosowsky & Stebbins 1997a; Seljak & Zaldarriaga 1997) . Inflation models predict the existence of a stochastic background of GW. A detection would provide the "smoking gun" for inflation. The amplitude of the GW in this background is directly proportional to the square of the energy scale of inflation, so that a detection of polarization would nail down key parameters of the inflationary model (e.g., Dodelson, Kinney, & Kolb 1997; Kinney 1998).

In this article we will review the mechanism by which polarization is generated and discuss what can be learned from measurements of polarization. In § 1.2 we will briefly review the physics of temperature anisotropies, although the reader is encouraged to go to one of the many reviews in the literature for further details. In § 1.3 we will discuss how polarization gets generated during recombination and to what it is sensitive. In § 1.4 we will discuss the imprint of GW. In § 1.5 we will review some of the physical processes that can affect the polarization signal after recombination. We conclude in § 1.6.

1.2 Temperature Anisotropies

In this section we will summarize the relevant facts about hydrogen recombination and temperature anisotropies. It is not our intention to provide an extensive review of these topics. The interested reader should consult other reviews (e.g., Hu & Dodelson 2002; Hu 2003). A discussion on the relevance of CMB studies for particle physics can be found in Kamionkowski & Kosowsky (1999).

1.2.1 Hydrogen Recombination and Thomson Scattering

The most abundant element in our Universe is hydrogen, and its ionization state has profound consequences on the CMB. The temperature of the CMB increased linearly with redshift, $T \propto (1+z)$. The interaction between the CMB photons and the hydrogen atoms kept

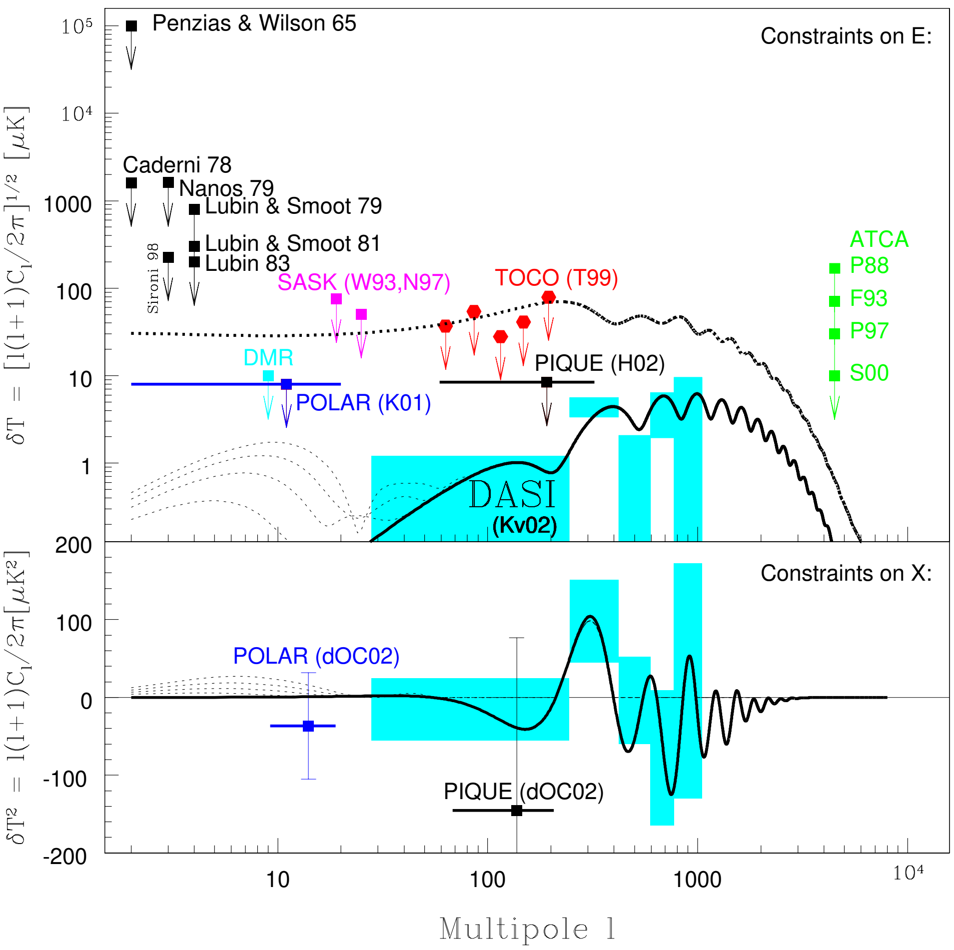

Fig. 1.1. Summary of polarization measurements and upper limits before the release of *WMAP* results, kindly provided by Angelica de Oliveira-Costa (adapted from de Oliveira-Costa et al. 2004). The top (bottom) panel shows results for the E (cross-correlation) power spectra.

hydrogen ionized until a redshift of $z \approx 1000$. At this time, corresponding to a conformal time of $\tau_R \approx 110\ (\Omega_m h^2)^{-1/2}$ Mpc, there are not enough energetic photons in the CMB to keep hydrogen ionized, so it recombines. Conformal time is defined by $a\, d\tau = dt$, with a the expansion factor and t the physical time. It is useful because a null geodesic is simply given by $d\tau = dx$, where x are comoving coordinates ($a\, dx = dr$, where r is the physical distance). For example the fact that $\tau_R \approx 110\ (\Omega_m h^2)^{-1/2}$ Mpc means a photon traveling on a straight line since the Big Bang until recombination would have traveled between two points that *today* are separated by a physical distance of $110\ (\Omega_m h^2)^{-1/2}$ Mpc.

The fraction of free electrons coming from hydrogen and helium is shown in Figure 1.2 (it was calculated using RECFAST of Seager, Sasselov, & Scott 1999). One of the main

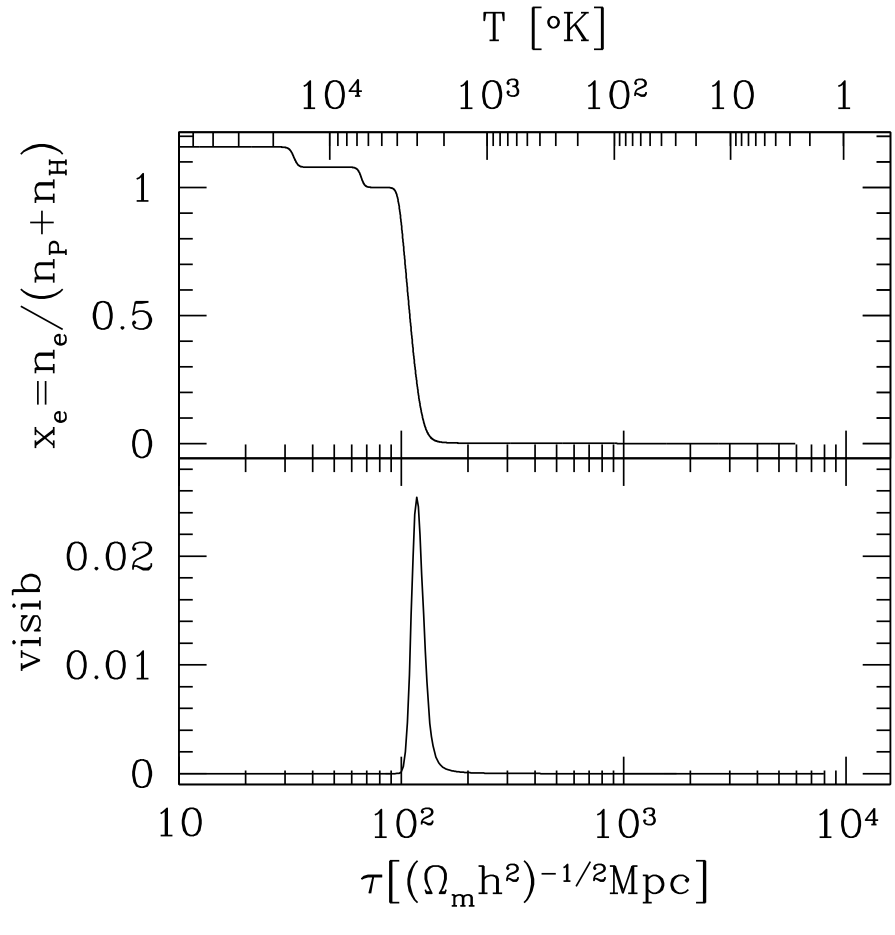

Fig. 1.2. In the top panel we show the ratio of number densities of free electrons and baryons. At early times the fraction is bigger than one because it includes electrons coming from helium. The bottom panel shows the visibility function that gives the probability a photon we observe last scattered at a particular position along the line of sight. The x-axis is labeled using conformal coordinates on the bottom and the temperature of the CMB on the top.

points to take away from the figure is that recombination happens rather fast. The width of recombination is $\delta\tau_R/\tau_R \approx 0.1-0.2$.

The other process we need to consider to understand how anisotropies are generated is Thomson scattering. When hydrogen is ionized the CMB photons can scatter with free electrons. This process conserves the number of photons and does not change their energy (because we are working in the limit of infinite electron mass). The mean free path for Thomson scattering in comoving Mpc is, $\lambda_T = (a n_e \sigma_T)^{-1} = 4$ Mpc $\frac{1}{x_e}(\frac{0.0125}{\Omega_b h^2})(\frac{0.9}{1-Y_p/2})(\frac{1000}{(1+z)})^2$, where n_e, x_e, and Y_p are the electron density, fraction of free electrons, and the primordial helium mass fraction, respectively.

Before recombination ($x_e \approx 1$) the mean free path was much smaller than the horizon at the time [$\tau_R \approx 110\,(\Omega_m h^2)^{-1/2}$ Mpc]. Photons were hardly able to travel without scattering, a regime called "tight coupling." After recombination ($x_e \approx 3 \times 10^{-4}$) the mean free path becomes much larger than the horizon, so photons can travel in a straight line to our detectors. The Universe has become transparent for CMB photons, a process also called decoupling.

In the bottom panel of Figure 1.2 we show the visibility function, which gives the probability a photon we observe last scattered at a particular position along the line of sight. The function is strongly peaked. After recombination the photons no longer scatter, so the visibility function is almost zero. Before recombination the scatterings were so frequent that for most photons the last scattering occurs right around recombination. Thus, the CMB photons are coming from a very narrow range in distance, given by the width of the last-scattering surface, $\delta\tau_R/\tau_R \approx 0.1$. The collection of these regions in all directions on the sky form a very thin sphere of radius $D_{LSS} = \tau_0 - \tau_R \approx 6000(\Omega h^2)^{-1/2}$Mpc, called the last-scattering surface (LSS).

1.2.2 *Review of Temperature Anisotropies*

Now we are in a position to understand the origin of the CMB anisotropies. There are several reasons why the temperature we observe in different directions is not exactly the same. Differences in the density of photons across the last-scattering surface will lead to differences in the observed intensity as a function of position on the sky. If the density of photons is higher in a particular region, we see this as a hot spot. These same density differences across the Universe lead to gravitational potential differences. If photons climb (go down) a potential well to get to us, they get redshifted (blueshifted), and this decreases (increases) the observed temperature. The gravitational potential differences create forces that cause motions, and these motions create shifts in frequency due to the Doppler effect. Thus, if photons come to us from a region that is moving toward (away from) us, they get blueshifted (redshifted), which we observe as a higher (lower) temperature. Finally, if the gravitational potentials are changing with time, the energy of photons changes along the way, leading to the so called integrated Sachs-Wolfe (ISW) effect (Sachs & Wolfe 1967). For a detailed discussion of all the relevant equations in both synchronous and conformal gauges, see Ma & Bertschinger (1995), and for more details as to how to treat polarization and GW, see Hu et al. (1998).

In the Newtonian gauge, the temperature fluctuations $\Delta_T = \delta T/T$ observed in direction $\hat{n}$ can be written as

$$(\Delta_T + \psi)(\hat{n}) = (\frac{\delta_\gamma}{4} + \psi)|_{\tau_R} + \hat{n}\cdot v_b|_{\tau_R} + \int d\tau' e^{-\kappa(\tau_0,\tau')}(\dot{\phi} + \dot{\psi}). \tag{1.1}$$

We have introduced $\delta_\gamma = \delta\rho_\gamma/\rho_\gamma$, the fractional energy density fluctuations in the CMB, v_b the baryon velocity, ϕ and ψ the two gravitational potentials in terms of which the metric fluctuations are given by $ds^2 = a^2(\tau)[-(1+2\psi)d\tau^2 + (1-2\phi)dx^2]$, and the optical depth $\kappa(\tau_2,\tau_1) = \int_{\tau_2}^{\tau_1} a n_e x_e d\tau$. The first term is usually referred to as the monopole contribution, while the second is the Doppler or dipole contribution.

In Equation 1.1 we have not included the terms coming from polarization because they are sub-dominant. We have approximated the visibility function by a δ-function; that is why the first two terms are evaluated at recombination. The different terms describe the physical effects mentioned above. From left to right, they correspond to photon energy density fluctuations, gravitational potential redshifts, Doppler shifts, and the ISW effect. Note that the ISW effect is an integral along the line of sight not constrained to recombination.

To be able to calculate the power spectrum of the anisotropies, we need to evaluate the different terms in Equation 1.1. Because we are dealing with small perturbations and linear theory, perturbations are usually expanded in Fourier modes, and the anisotropies are calculated for each Fourier mode individually. The contributions of individual modes are then added to calculate the power spectrum.

As discussed in the previous section, before recombination Thomson scattering was very efficient. As a result it is a good approximation to treat photons and baryons as a single fluid. This treatment is called the tight-coupling approximation and will allow us to evolve the perturbations until recombination to calculate the different terms in Equation 1.1.

The equation for the photon density perturbations for one Fourier mode of wavenumber k is that of a forced and damped harmonic oscillator (e.g., Seljak 1994; Hu & Sugiyama 1995):

$$\begin{aligned} \ddot{\delta_\gamma} + \frac{\dot{R}}{(1+R)}\dot{\delta_\gamma} + k^2 c_s^2 \delta_\gamma &= F \\ F &= 4[\ddot{\phi} + \frac{\dot{R}}{(1+R)}\dot{\phi} - \frac{1}{3}k^2\psi] \\ \dot{\delta_\gamma} &= -\frac{4}{3}kv_\gamma + 4\dot{\phi}. \end{aligned} \tag{1.2}$$

The photon-baryon fluid can sustain acoustic oscillations. The inertia is provided by the baryons, while the pressure is provided by the photons. The sound speed is $c_s^2 = 1/3(1+R)$, with $R = 3\rho_b/4\rho_\gamma = 31.5\ (\Omega_b h^2)(T/2.7)^{-4}[(1+z)/10^3]^{-1}$. As the baryon fraction goes down, the sound speed approaches $c_s^2 \rightarrow 1/3$. The third equation above is the continuity equation.

As a toy problem, we will solve Equation 1.2 under some simplifying assumptions. If we consider a matter-dominated universe, the driving force becomes a constant, $F = -4/3k^2\psi$, because the gravitational potential remains constant in time. We neglect anisotropic stresses so that $\psi = \phi$, and, furthermore, we neglect the time dependence of R. Equation 1.2 becomes that of a harmonic oscillator that can be trivially solved. This is a very simplified picture, but it captures most of the relevant physics we want to discuss. More elaborate approximation schemes can be found in the literature. They allow the calculation of the power spectrum with an accuracy of roughly 10% (Seljak 1994; Hu & Sugiyama 1995; Weinberg 2001a,b; Mukhanov 2003).

To obtain the final solution we need to specify the initial conditions. We will restrict ourselves to adiabatic initial conditions, the most natural outcome of inflation. In our context this means that initially $\phi = \psi = \phi_0$, $\delta_\gamma = -8/3\phi_0$, and $v_\gamma = 0$. We have denoted ϕ_0 the initial amplitude of the potential fluctuations. We will take ϕ_0 to be a Gaussian random variable with power spectrum P_{ϕ_0}.

We have made enough approximations that the evaluation of the sources in the integral solution has become trivial. The solution for the density and velocity of the photon fluid at recombination are:

$$(\frac{\delta_\gamma}{4} + \psi)|_{\tau_R} = \frac{\phi_0}{3}(1+3R)\cos(kc_s\tau_R) - \phi_0 R$$

$$v_\gamma|_{\tau_R} = -\phi_0(1+3R)c_s\sin(kc_s\tau_R). \tag{1.3}$$

Equation 1.3 is the solution for a single Fourier mode. All quantities have an additional spatial dependence ($e^{i\mathbf{k}\cdot\mathbf{x}}$), which we have not included to make the notation more compact. With that additional term the solution of Equation 1.1 becomes

$$\begin{aligned} \Delta_T(\hat{n}) &= e^{ikD_{LSS}\cos\theta} S \\ S &= \phi_0 \frac{(1+3R)}{3}[\cos(kc_s\tau_R) - \frac{3R}{(1+3R)} \\ &\quad -i\sqrt{\frac{3}{1+R}}\cos\theta\sin(kc_s\tau_R)], \end{aligned} \tag{1.4}$$

where we have neglected the ψ on the left-hand side because it is a constant independent of $\hat{n}$. We have also ignored the ISW contribution. We have introduced $\cos\theta$, the cosine of the angle between the direction of observation and the wavevector k; for example, $k\cdot x = kD_{LSS}\cos\theta$. The term proportional to $\cos\theta$ is the Doppler contribution.

Once the temperature perturbation produced by one Fourier mode has been calculated, we need to expand it into spherical harmonics to calculate the $a_{lm} = \int d\Omega\ Y^*_{lm}(\hat{n})\ \Delta T(\hat{n})$. The power spectrum of temperature anisotropies is expressed in terms of the a_{lm} coefficients as $C_{Tl} = \sum_m |a_{lm}|^2$. The contribution to C_{Tl} from each Fourier mode is weighted by the amplitude of primordial fluctuations in this mode, characterized by the power spectrum of ϕ_0, $P_{\phi_0} = Ak^{n-4}$. We will take the power-law index to be $n=1$ in our approximate formulas. In practice, fluctuations on angular scale l receive most of their contributions from wavevectors around $k^* = l/D_{LSS}$, so roughly the amplitude of the power spectrum at multipole l is given by the value of the sources in Equation 1.3 at k^*.

After summing the contributions from all modes, the power spectrum is roughly given by

$$\begin{aligned} l(l+1)C_{Tl} \approx\ & A\{[\frac{(1+3R)}{3}\cos(k^*c_s\tau_R) - R]^2 + \\ & \frac{(1+3R)^2}{3}c_s^2\sin^2(k^*c_s\tau_R)\}. \end{aligned} \tag{1.5}$$

Equation 1.5 can be used to understand the basic features in the CMB power spectra shown in Figure 1.3. The baryon drag on the photon-baryon fluid reduces its sound speed below $1/3$ and makes the monopole contribution dominant [the one proportional to $\cos(k^*c_s\tau_R]$. Thus, the C_{Tl} spectrum peaks where the monopole term peaks, $k^*c_s\tau_R = \pi, 2\pi, 3\pi, \cdots$, which correspond to $l_{peak} = n\pi D_{LSS}/c_S\tau_R$. More detailed discussions of the physics of the acoustic peaks can be found in reviews such as that by Hu & Dodelson (2002) or Hu (2003).

It is very important to understand the origin of the acoustic peaks. In this model the Universe is filled with standing waves; all modes of wavenumber k are in phase, which leads to the oscillatory terms. The sine and cosine in Equation 1.5 originate in the time dependence of the modes. Each mode l receives contributions preferentially from Fourier modes of a particular wavelength k^* (but pointing in all directions), so to obtain peaks in C_l, it is crucial that all modes of a given k are in phase. If this is not the case, the features in the C_{Tl} spectra will be blurred and can even disappear. This is what happens when one considers the spectra produced by topological defects (e.g., Pen, Seljak, & Turok 1997). The phase coherence of

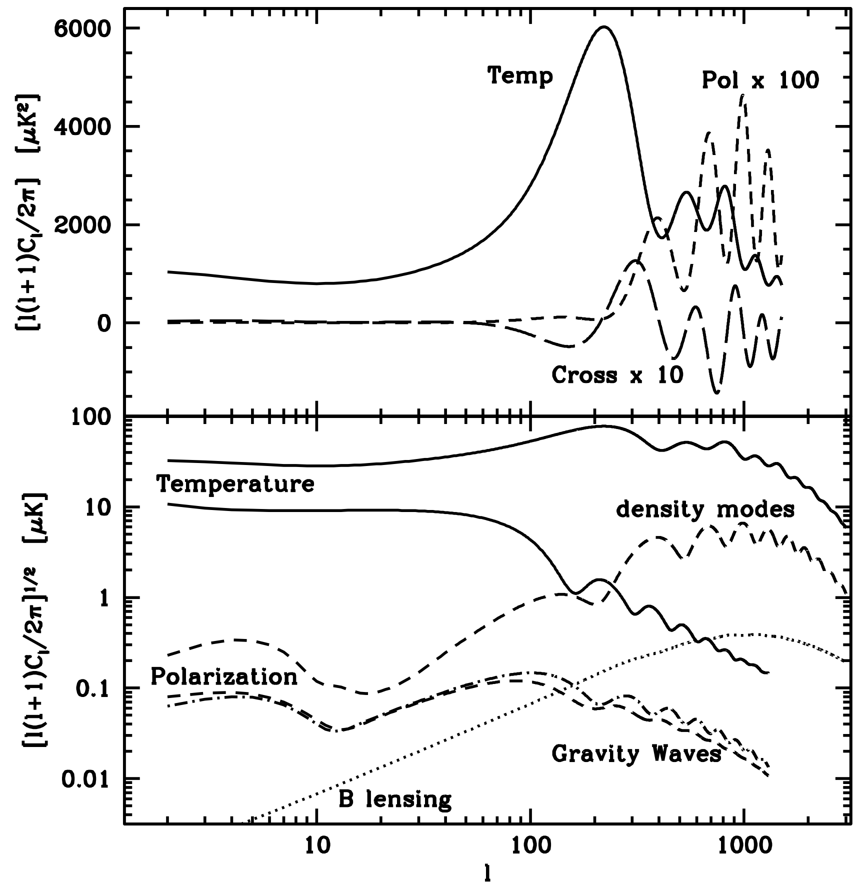

Fig. 1.3. Temperature, polarization, and cross-correlation power spectrum produced by density perturbations in the fiducial ΛCDM model ($\Omega_m = 0.3$, $\Omega_\Lambda = 0.7$, $h = 0.7$, $\Omega_b h^2 = 0.02$). For display purposes the polarization (cross-correlation) power spectrum was multiplied by a factor of 100 (10).

all modes of a given wavenumber can be traced to the fact that perturbations were produced very early on and had wavelengths larger than the horizon during many expansion times.

There are additional physical effects we have neglected. The Universe was radiation dominated early on, and modes of wavelength smaller and bigger than the horizon at matter-radiation equality behave differently. During the radiation era the perturbations in the photon-baryon fluid are the main source for the gravitational potentials which decay once a mode enters into the horizon. The gravitational potential decay acts as a driving force for the oscillator in Equation 1.2, so a feedback loop is established. As a result, the acoustic oscillations for modes that entered the horizon before matter-radiation equality have a higher amplitude. In the C_{Tl} spectrum the separation between modes that experience this feedback and those that do not occur at $l \sim D_{LSS}/\tau_{eq}$, where $\tau_{eq} \approx 16(\Omega_m h^2)^{-1}$ Mpc is the conformal time of matter-radiation equality. Larger l values receive their contributions from modes that entered the horizon before matter-radiation equality. Finally, when a mode is inside the horizon during the radiation era the gravitational potentials decay.

There is a competing effect, Silk damping (Silk 1968), that reduces the amplitude of the large-l modes. The photon-baryon fluid is not a perfect fluid. Photons have a finite mean free path and thus can random walk away from the peaks and valleys of the standing waves. Thus, perturbations of wavelength comparable to or smaller than the distance the photons can random walk get damped. This effect can be modeled by multiplying Equation 1.4 by $\exp(-k^2/k_s^2)$, with $k_s^{-1} \propto \tau_R^{1/2}(\Omega_b h^2)^{-1/2}$. Silk damping is important for multipoles of order $l_{Silk} \sim k_s D_{LSS}$.

Finally, the last-scattering surface has a finite width (Fig. 1.2). Perturbations with wavelength comparable to this width get smeared out due to cancellations along the line of sight. This effect introduces an additional damping with a characteristic scale $k_w^{-1} \propto \delta\tau_R$.

1.3 Polarization

In this section we will describe how polarization is characterized and how it is generated by density perturbations. We will stress the similarities and differences with temperature anisotropies. We will focus on polarization generated by density perturbations and leave the signal of GW for a later section. The physics of polarization has been previously reviewed in Hu & White (1997), Kosowsky (1999), and Hu (2003).

1.3.1 Characterizing the Radiation Field

The aim of this part is to summarize the mathematical tools needed to describe the CMB anisotropies. The anisotropy field is characterized by a 2×2 intensity tensor I_{ij}. For convenience, we normalize this tensor so it represents the fluctuations in units of the mean intensity ($I_{ij} = \delta I/I_0$). The intensity tensor is a function of direction on the sky, $\hat{n}$, and two directions perpendicular to $\hat{n}$ that are used to define its components ($\hat{\mathbf{e}}_1$,$\hat{\mathbf{e}}_2$). The Stokes parameters Q and U are defined as $Q = (I_{11} - I_{22})/4$ and $U = I_{12}/2$, while the temperature anisotropy is given by $T = (I_{11}+I_{22})/4$ (the factor of 4 relates fluctuations in the intensity with those in the temperature, $I \propto T^4$). When representing polarization using "rods" in a map, the magnitude is given by $P = \sqrt{Q^2+U^2}$, and the orientation makes an angle $\alpha = \frac{1}{2}\arctan(U/Q)$ with $\hat{\mathbf{e}}_1$. In principle the fourth Stokes parameter V that describes circular polarization is needed, but we ignore it because it cannot be generated through Thomson scattering, so the CMB is not expected to be circularly polarized. While the temperature is invariant under a right-handed rotation in the plane perpendicular to direction $\hat{n}$, Q and U transform under rotation by an angle ψ as

$$(Q \pm iU)'(\hat{n}) = e^{\mp 2i\psi}(Q \pm iU)(\hat{n}), \tag{1.6}$$

where $\hat{\mathbf{e}}_1' = \cos\psi\,\hat{\mathbf{e}}_1 + \sin\psi\,\hat{\mathbf{e}}_2$ and $\hat{\mathbf{e}}_2' = -\sin\psi\,\hat{\mathbf{e}}_1 + \cos\psi\,\hat{\mathbf{e}}_2$. The quantities $Q \pm iU$ are said to be spin 2.

We already mentioned that the statistical properties of the radiation field are usually described in terms the spherical harmonic decomposition of the maps. This basis, basically the Fourier basis, is very natural because the statistical properties of anisotropies are rotationally invariant. The standard spherical harmonics are not the appropriate basis for $Q \pm iU$ because they are spin-2 variables, but generalizations (called ${}_{\pm 2}Y_{lm}$) exist. We can expand

$$(Q \pm iU)(\hat{n}) \quad = \quad \sum_{lm} a_{\pm 2,lm} \; {}_{\pm 2}Y_{lm}(\hat{n}). \tag{1.7}$$

Q and U are defined at each direction $\hat{n}$ with respect to the spherical coordinate system $(\hat{\mathbf{e}}_\theta, \hat{\mathbf{e}}_\phi)$ (Kamionkowski, Kosowsky, & Stebbins, 1997b; Zaldarriaga & Seljak 1997). To ensure that Q and U are real, the expansion coefficients must satisfy $a^*_{-2,lm} = a_{2,l-m}$. The equivalent relation for the temperature coefficients is $a^*_{T,lm} = a_{T,l-m}$.

Instead of $a_{\pm 2,lm}$, it is convenient to introduce their linear combinations $a_{E,lm} = -(a_{2,lm} + a_{-2,lm})/2$ and $a_{B,lm} = i(a_{2,lm} - a_{-2,lm})/2$ (Newman & Penrose 1966). We define two quantities in real space, $E(\hat{n}) = \sum_{l,m} a_{E,lm}\, Y_{lm}(\hat{n})$ and $B(\hat{n}) = \sum_{l,m} a_{B,lm}\, Y_{lm}(\hat{n})$. E and B completely specify the linear polarization field.

The temperature is a scalar quantity under a rotation of the coordinate system, $T'(\hat{n}' = \mathcal{R}\hat{n}) = T(\hat{n})$, where $\mathcal{R}$ is the rotation matrix. We denote with a prime the quantities in the transformed coordinate system. While $Q \pm iU$ are spin 2, $E(\hat{n})$ and $B(\hat{n})$ are invariant under rotations. Under parity, however, E and B behave differently, E remains unchanged, while B changes sign.

As an illustration, in Figure 1.4 we show polarization patterns that have positive and negative E and B. It is clear that B patterns are "curl-like," having different properties than the E patterns under parity transformation. When reflected across a line going through the center, the E patterns remain unchanged, whereas the B patterns change from positive to negative. We want to stress at this point that whether a polarization field has an E or B component is a property of the pattern of polarization rods *around* a particular point, and not at the point itself. In this sense E and B are not local quantities.

There is a clear analogy between vector fields and polarization fields with regard to their geometrical properties. The polarization field is a spin-2 field, which means that if one rotates the coordinate system by 180° one goes back to the same components of the field, as opposed to 360° needed for vector fields. However, conceptually things are very similar, with E and B playing the roles of the gradient and curl parts. See Bunn et al. (2003) for a more detailed description of similarities and differences between vectors and polarization fields.

To characterize the statistics of the CMB perturbations, only four power spectra are needed, those for T, E, B and the cross correlation between T and E. The cross correlation between B and E or B and T vanishes if there are no parity-violating interactions because B has the opposite parity to T or E. Examples of models where this is not true were presented in Lue, Wang, & Kamionkowski (1999). The power spectra are defined as the rotationally invariant quantities $C_{Tl} = \frac{1}{2l+1}\sum_m \langle a^*_{T,lm} a_{T,lm}\rangle$, $C_{El} = \frac{1}{2l+1}\sum_m \langle a^*_{E,lm} a_{E,lm}\rangle$, $C_{Bl} = \frac{1}{2l+1}\sum_m \langle a^*_{B,lm} a_{B,lm}\rangle$, and $C_{Cl} = \frac{1}{2l+1}\sum_m \langle a^*_{T,lm} a_{E,lm}\rangle$. The brackets $\langle \cdots \rangle$ denote ensemble averages.

We will not discuss how to define correlation functions in real space for the polarization field. The reader is referred to the literature (e.g., Kamionkowski et al. 1997b; Zaldarriaga 1998; Tegmark & de Oliveira-Costa 2001). We only want to point out that the spin nature of the Stokes parameters needs to be considered to properly define correlation functions.

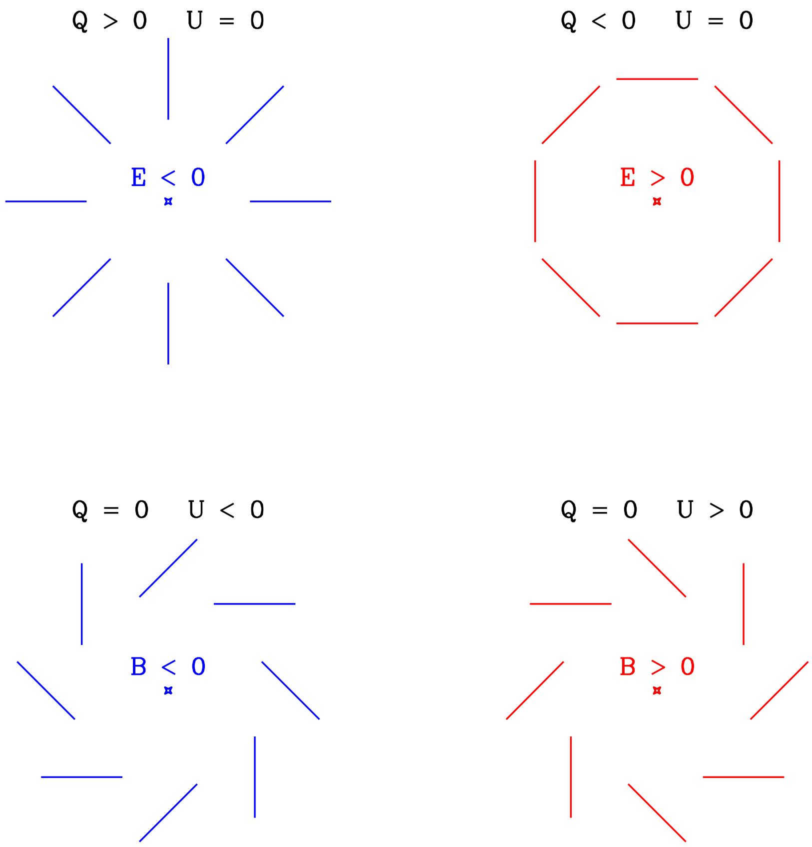

Fig. 1.4. Example of E-type and B-type patterns of polarization. Note that if reflected across a line going through the center the E patterns are unchanged, while the B patterns switch with one another.

1.3.2 The Physics of Polarization

Polarization is generated by Thomson scattering between photons and electrons, which means that polarization cannot be generated after recombination (except for reionization, which we will discuss later). But Thomson scattering is not enough. The radiation incident on the electrons must also be anisotropic. In fact, its intensity needs to have a quadrupole moment. This requirement of having both Thomson scattering and anisotropies is what makes polarization relatively small. After recombination, anisotropies grow by free streaming, but there are no scattering to generate polarization. Before recombination there were so many scatterings that they erased any anisotropy present in the photon-baryon fluid.

In the context of anisotropies induced by density perturbations, velocity gradients in the photon-baryon fluid are responsible for the quadrupole that generates polarization. Let us consider a scattering occurring at position x_0: the scattered photons came from a distance of order the mean free path (λ_T) away from this point. If we are considering photons traveling in direction $\hat{n}$, they roughly come from $x = x_0 + \lambda_T \hat{n}$. The photon-baryon fluid at that point was moving at velocity $v(x) \approx v(x_0) + \lambda_T \hat{n}_i \partial_i v(x_0)$. Due to the Doppler effect the temperature seen by the scatterer at x_0 is $\delta T(x_0, \hat{n}) = \hat{n} \cdot [v(x) - v(x_0)] \approx \lambda_T \hat{n}_i \hat{n}_j \partial_i v_j(x_0)$, which is quadratic in $\hat{n}$ (i.e., it has a quadrupole). *Velocity gradients in the photon-baryon fluid lead to a quadrupole component of the intensity distribution, which, through Thomson scattering, is converted into polarization.*

The polarization of the scattered radiation field, expressed in terms of the Stokes parameters Q and U, is given by $(Q + iU) \propto \sigma_T \int d\Omega' (\mathbf{m} \cdot \hat{\mathbf{n}}')^2 T(\hat{\mathbf{n}}') \propto \lambda_p \mathbf{m}^i \mathbf{m}^j \partial_i v_j|_{\tau_R}$, where σ_T is the Thomson scattering cross-section and we have written the scattering matrix as $P(\mathbf{m}, \hat{\mathbf{n}}') = -3/4 \sigma_T (\mathbf{m} \cdot \hat{\mathbf{n}}')^2$, with $\mathbf{m} = \hat{\mathbf{e}}_1 + i\hat{\mathbf{e}}_2$. In the last step, we integrated over all directions of the incident photons $\hat{\mathbf{n}}'$. As photons decouple from the baryons, their mean free path grows very rapidly, so a more careful analysis is needed to obtain the final polarization* (Zaldarriaga & Harari 1995):

$$(Q + iU)(\hat{\mathbf{n}}) \approx \epsilon \delta\tau_R \mathbf{m}^i \mathbf{m}^j \partial_i v_j|_{\tau_R}, \tag{1.8}$$

where $\delta\tau_R$ is the width of the last-scattering surface and is giving a measure of the distance photons travel between their last two scatterings, and ϵ is a numerical constant that depends on the shape of the visibility function. The appearance of $\mathbf{m}^i \mathbf{m}^j$ in Equation 1.8 assures that $(Q + iU)$ transforms correctly under rotations of $(\hat{\mathbf{e}}_1, \hat{\mathbf{e}}_2)$.

If we evaluate Equation 1.8 for each Fourier mode and combine them to obtain the total power, we get the equivalent of Equation 1.5,

$$l(l+1) C_{El} \approx A \epsilon^2 (1 + 3R)^2 (k^* \delta\tau_R)^2 \sin^2(k^* c_s \tau_R), \tag{1.9}$$

where we are assuming $n = 1$ and that l is large enough that factors like $(l+2)!/(l-2)! \approx l^4$. The extra k^* in Equation 1.9 originates in the gradient in Equation 1.8. As will be discussed later, density perturbations produce no B, so only three power spectra are needed to characterize the maps.

The curves in Figure 1.3 illustrate the differences between temperature and polarization power spectra. The large-angular scale polarization is greatly suppressed by the $k\delta\tau_R$ factor. Correlations over large angles can only be created by the long-wavelength perturbations, but these cannot produce a large polarization signal because of the tight coupling between photons and electrons prior to recombination. Multiple scatterings make the plasma very homogeneous; only wavelengths that are small enough to produce anisotropies over the mean free path of the photons will give rise to a significant quadrupole in the temperature distribution, and thus to polarization. Wavelengths much smaller than the mean free path decay due to photon diffusion (Silk damping) and so are unable to create a large quadrupole and polarization. As a result polarization peaks at the scale of the mean free path.

On sub-degree angular scales, temperature, polarization, and the cross-correlation power spectra show acoustic oscillations (Fig. 1.3). In the polarization and cross-correlation spectra the peaks are much sharper. The polarization is produced by velocity gradients of the photon-baryon fluid at the last-scattering surface (Equ. 1.8). The temperature receives contributions from density and velocity perturbations (Equ. 1.5), and the oscillations in each

* The velocity in this equation is in the conformal gauge.

partially cancel one another, making the features in the temperature spectrum less sharp. The dominant contribution to the temperature comes from the oscillations in the density (Equ. 1.3), which are out of phase with the velocity. This explains the difference in location between the temperature and polarization peaks. The extra gradient in the polarization signal, Equation 1.8, explains why its overall amplitude peaks at a smaller angular scale.

1.3.3 The Information Encoded in the Polarization Generated at the LSS

Now that we have reviewed the physics at recombination, we consider what can be learned from a measurement of polarization on sub-degree angular scales. The temperature and polarization anisotropies produced by density perturbations are characterized by three power spectra. Once polarization is measured, we have two extra sources of information from which to extract constraints on parameters. Although constraints should get tighter in principle, in practice because polarization anisotropies are significantly smaller than temperature ones, and thus more difficult to detect, parameter constraints do not improve that much from the measurement of the polarization. This is specially true if we restrict ourselves to the standard cosmological parameters such as those describing the matter content of the Universe, but not necessarily true for others or when some degeneracies are considered (Zaldarriaga et al. 1997; Eisenstein et al. 1999). This fact can be viewed in two different ways. One could say that a measurement of polarization in the acoustic peak region is not as relevant because it would not dramatically alter our constraints on parameters. Alternatively, one could say that it will provide a consistency check because, once the parameters of the model are determined from the temperature anisotropies, polarization is accurately predicted. We should keep in mind that, although everything seems to be falling in line with theoretical predictions, there are remarkably few real consistency checks, when the same quantity is measured accurately in two independent ways. We will mention three consistency checks that can be performed using polarization on sub-degree angular scales.

In what is quickly becoming the standard model, perturbations are generated during a period of inflation. The potential of CMB anisotropies to test inflationary models has long been recognized (e.g., Hu & White 1996; Hu, Spergel, & White 1997). One of the main predictions of inflation is that perturbations are correlated over scales larger than the horizon at recombination and that modes have phase coherence, which leads to the peaks in the power spectrum. Because the speed of the acoustic waves is smaller than the speed of light, one can produce the acoustic peaks in the temperature and polarization spectra without resorting to above-horizon perturbations (e.g., Turok 1996a, b). Moreover, because temperature can be produced after recombination (when the horizon is bigger) through the ISW effect, correlations on scales larger than two degrees (the scale of the recombination horizon) are not proof of above-horizon perturbations. Correlations of the polarization, on the other hand, provide a clearer test because there is no equivalent to the ISW effect (Spergel & Zaldarriaga 1997). This test has now been performed by the *WMAP* team, further strengthening the case for inflation (Pieris et al. 2003)

It is customary to assume that the power spectrum of primordial fluctuations is a simple power law, perhaps with a logarithmically varying spectral index. Although this is well motivated in the context of inflation, it should be checked. Moreover, preliminary determinations of the power spectrum, combining results from *WMAP* and large-scale structure, hint that something strange may be going on. Constraints on the power spectrum of primordial fluctuations come from comparing the amplitude of temperature perturbations at different angular scales. At least some of the changes produced by differences in the primordial spectrum can be mimicked by changes in the cosmological parameters. If both temperature and polarization are measured, there are three independent measures of the level of fluctuations on each scale. Moreover, temperature and polarization depend differently on cosmological parameters. Thus, the simultaneous measurement of temperature and polarization can be used to separate the early (inflation era) and later Universe physics affecting the CMB (e.g., Tegmark & Zaldarriaga 2002).

In the simplest inflationary models, perturbations only come in the adiabatic form. However, in more complicated inflationary models or in other classes of early-universe "scenarios," isocurvature perturbations can arise. In a model with photons, baryons, neutrinos and cold dark matter, there are actually four isocurvature modes in addition to the adiabatic one (e.g., Bucher, Moodley, & Turok 2000; Rebhan & Schwarz 1994; Challinor & Lasenby 1999). The simultaneous measurement of temperature and polarization will allow us to put constraints on small admixtures of these components that would be impossible otherwise (Bucher, Moodley, & Turok 2001).

Finally, because polarization perturbations are accurately predicted once temperature is measured, polarization can be used to make several consistency checks on the way recombination happened. In particular, changes in fundamental constants such as the fine structure constant, the gravitational constant, the speed at which the Universe was expanding during recombination, or the presence of ionizing photons on top of those from the CMB should be severely constrained once the data are in (Kaplinghat, Scherrer, & Turner 1999; Peebles, Seager, & Hu 2000; Hannestad & Scherrer 2001; Landau, Harari, & Zaldarriaga 2001; Uzan 2003; Zahn & Zaldarriaga 2003).

1.4 The $E-B$ Decomposition and the Imprint of Gravity Waves

The study of the anisotropies produced by GW has a long history (e.g., Polnarev 1985; Crittenden, Davis, & Steinhardt 1993; Coulson, Crittenden, & Turok 1994; Crittenden, Coulson, & Turok 1995). Perhaps the biggest driving force behind the push to measure polarization is the possibility of detecting a stochastic background of GW. The same mechanism that creates the seeds for structure formation, the stretching of vacuum fluctuations during inflation, is also expected to generate a stochastic background of GW. The amplitude of the GW in the background is directly proportional to the Hubble constant during inflation, or equivalently the square of energy scale of inflation.

As photons travel in the metric perturbed by a GW [$ds^2 = a^2(\tau)\ [-d\tau^2 + (\delta_{ij} + h^T_{ij})dx^i dx^j]$], they get redshifted or blueshifted depending on their direction of propagation relative to the direction of propagation of the GW and the polarization of the GW. For example, for a GW traveling along the z axis, the frequency shift is given by $\frac{1}{\nu}\frac{d\nu}{d\tau} = \frac{1}{2}\ \hat{n}^i \hat{n}^j \dot{h}^{T(\pm)}_{ij} = \frac{1}{2}\ (1 - \cos^2\theta) e^{\pm i2\phi}\ \ \dot{h}_t\ \exp(ik \cdot x)$, where (θ, ϕ) describe the direction of propagation of the photon, the $\pm$ correspond to the different polarizations of the GW, and h_t gives the time-dependent amplitude of the GW. During the matter-dominated era, for example, $h_t = 3 j_1(k\tau)/k\tau$. This effect is analogous to the ISW effect: time changes in the metric lead to frequency shifts (or equivalently shifts in the temperature of the black body spectrum). Notice that the angular dependence of this frequency shift is quadrupolar in nature. As a result, the temperature fluctuations induced by this effect as photons travel between successive scatterings before recombination produce a quadrupole intensity distribution, which, through Thomson scattering, lead to polarization. *We want to stress that polarization is always generated by Thom-*

son scatterings, whether we talk about polarization generated by density perturbations or by GW. All that differs in these two cases is what is responsible for the quadrupole anisotropies.

Figure 1.3 shows the temperature and polarization anisotropy power spectrum produced by GW. We have arbitrarily normalized the GW contribution so that the ratio of $l = 2$ contributions from tensors and density perturbations $T/S \approx 0.1$, corresponding to an energy scale of inflation, $E_{\rm inf} \approx 2 \times 10^{16}\,\mathrm{GeV}$. The temperature power spectrum, produced mainly after recombination, is roughly flat up to $l \approx 100$, and then rapidly falls off. By contrast, polarization is produced at recombination (except for the reionization bump at low values of l, to be discussed later). The power spectrum of polarization peaks at $l \approx 100$ because, just as for density perturbation, GW much larger than the mean free path of the photons at decoupling cannot generate an appreciable quadrupole. The spectrum falls on small scales as well because the amplitude of GW decays when they enter the horizon, as they redshift away. The decay occurs at horizon crossing, much before the Silk damping scale.

So far we have ignored the spin 2 nature of polarization. Both E and B power spectrum are generated by GW (Kamionkowski et al. 1997a; Seljak & Zaldarriaga 1997). The current push to improve polarization measurements follows from the fact that density perturbations, to linear order in perturbation theory, cannot create any B-type polarization. As a rough rule of thumb, the amplitude of the peak in the B-mode power spectrum for GW is $[l(l+1)C_{Bl}/2\pi]^{1/2} = 0.024(E_{\rm inf}/10^{16}\mathrm{GeV})^2\mu\mathrm{K}$.

One can understand why GW can produce B, while density perturbations cannot, by analyzing the symmetries of the problem. We recall that we are dealing with a linear problem, so one Fourier mode of density perturbations or a single GW needs to be analyzed. When calculating the temperature and polarization maps that would be observed in a universe with a single Fourier mode of the density, one realizes that the problem has two symmetries. There is symmetry of rotation around the k vector and symmetry of reflection along any plane that contains the k vector. The pattern of polarization produced by this mode has to respect these two symmetries, which in turn implies that there cannot be any B modes generated in this case. In Figure 1.4, if the cross represents the tip of the k vector, it is clear that only the E patterns respect the symmetries. For one polarization of the GW, these symmetries are not satisfied, as is obvious from the pattern of redshifts they produce, $\frac{1}{\nu}\frac{d\nu}{d\tau} \propto \frac{1}{2}\,(1-\cos^2\theta)e^{\pm i2\phi}$. Gravitational waves can produce a B pattern.

1.5 After Recombination

In this section we will discuss a few different effects that can change the polarization pattern after recombination.

1.5.1 Reionization

So far we have ignored the fact that hydrogen became ionized when the first sources of UV radiation started shining. The exact time and way this happened is not yet fully understood, the recent results from *WMAP* indicate that reionization started pretty early, with a prefer value of $z \approx 20$ (Bennett et al. 2003). There are also indications from studies of absorption toward high-redshift quasars that something happened around redshift $z \approx 6-8$ (Fan et al. 2002). It could well be that reionization is not a one-stage process. Depending on the details of the sources of radiation, a more complicated ionization history could have occurred (e.g., Wyithe & Loeb 2003).

In any event, at these redshifts the density of hydrogen was so much lower than at recombination that even though hydrogen is fully ionized the optical depth is still relatively low; somewhere around 17% is what *WMAP* favors. Even though only a fraction of the photons scatter after recombination, this still has a dramatic effect on polarization on large angular scales, of order 10 degrees. On these scales the polarization produced at recombination is minimal because these scales are much larger than the mean free path at recombination. As can be seen in Figure 1.3, polarization has a power-law decay toward large scales.

After recombination, photons were able to travel a significant distance over which the large-wavelength modes can induce a quadrupole. This quadrupole leads to a bump in the polarization power spectrum shown in Figure 1.3 that is orders of magnitude higher than what polarization would be if it were not for reionization (e.g., Zaldarriaga 1997). If there were no reionization the power law decay would continue up to $l = 2$.

A detection of this large-scale signal will allow a precise measurement of the total optical depth and provide some additional information on how and when reionization happened. The height of the reionization bump is proportional to the total optical depth, while the shape and location of the peak contains information about when reionization happened (Zaldarriaga 1997; Kaplinghat et al. 2003a). The total amount of information that can be extracted is, however, limited because at these large scales there are only a few multipoles that one can measure (i.e., cosmic variance is large; e.g., Hu & Holder 2003). However, a measurement of the optical depth is very important because it breaks degeneracies between determinations of several parameters (Zaldarriaga et al. 1997; Eisenstein et al. 1999). This excess of large-scale polarization is what *WMAP* used to determine a redshift of reionization around $z \approx 20$ (Spergel et al. 2003).

1.5.2 Weak Lensing

As photons propagate from the last-scattering surface they get gravitationally deflected by mass concentrations, the large-scale structure of the Universe. This gravitational lensing effect changes both temperature and polarization anisotropies (e.g., Seljak 1996; Bernardeau 1997, 1998; Hu 2000), but has rather profound consequences for the pattern of CMB polarization. Even a polarization pattern that did not have any B component at recombination will acquire some B due to gravitational lensing (Zaldarriaga & Seljak 1998). The effect is simple to understand. Because of lensing, a photon originally traveling in direction $\hat{n}$ will be observed toward direction $\hat{n}'$. We can use the analogy with a vector field and assume we start with the pattern that is a perfect gradient. As vectors are slightly shifted around due to lensing, the field will develop a curl component.

In Figure 1.3 we show the B component generated by lensing of the E mode. It is clear from the figure that if the level of the GW background is much lower than shown there, then the lensing signal would be larger at almost all scales. Note that the lensing B does not have the reionization bump at low l. This is so because the power is actually coming from "aliasing" of the small-scale polarization power rather than from a rearrangement of the original large-scale power.

The ultimate limitation for detecting the stochastic background of GW comes form the spurious B modes generated by lensing. The lensing distortions to the temperature and polarization maps make them non-Gaussian (e.g., Bernardeau 1997, 1998; Zaldarriaga 2000; Cooray & Hu 2001; Okamoto & Hu 2002). Methods have been developed to use this non-Gaussianity to measure the projected mass density (Seljak & Zaldarriaga 1999a; Zaldarriaga & Seljak 1999; Hu 2001a,b; Okamoto & Hu 2002), which can be used to clean, at least partially, this contamination. With the methods proposed so far, the lowest energy scale that seems measurable is $E_{\rm inf} = 2 \times 10^{15}$ GeV (Kesden, Cooray, & Kamionkowski 2002; Knox & Song 2002). The energy scale of inflation is at present only very loosely constrained, so it is perfectly possible that the GW background is too small to be observed. However, if inflation is related to the Grand Unification scale around 10^{16} GeV, then there is a good chance that the GW background will be detected.

The lensing effect is not only a nuisance for detecting GW; it is interesting to constraint the large-scale structure that is doing the lensing. Because the last-scattering surface is at such high redshift, lensing of the CMB may eventually provide one of the deepest probes for large-scale structure. The level of structure on scales of order $2-1000$ Mpc at redshifts from $z \approx 10$ to $z \approx 0$ may eventually be constrained with this technique (e.g., Zaldarriaga & Seljak 1999). Lensing will not only allow a measurement of the level of fluctuations but may lead to actual reconstructed maps of the projected mass density that can be correlated with maps produced by CMB experiments and other probes (e.g., Goldeberg & Spergel 1999; Seljak & Zaldarriaga 1999b; Spergel & Goldberg 1999; Van Waerbeke, Bernardeau, & Benabed 2000; Benabed, Bernardeau, & van Waerbeke 2001; Song et al. 2003) and to strong constraints on parameters such as the mass of the neutrinos (Kaplinghat, Knox, & Song 2003b). On small scales, large mass concentrations such as cluster may leave a detectable signature (Seljak & Zaldarriaga 2000).

1.5.3 Foregrounds

As we have discussed, a significant amount of information is encoded in the large-scale polarization. The ability of polarization to determine the reionization history and with that help break some of the degeneracies between cosmological parameters relies on the large scales (Zaldarriaga et al. 1997).

Measuring polarization over the whole sky might be a problem when it comes to foregrounds. First, it means that one may have to use patches of the sky that are not that foreground free. Second, it appears that at least for the unpolarized component galactic foregrounds have rather red spectra, affecting large scales the most.

At microwave frequencies synchrotron, free-free, and dust emission are foreground contaminants. At present we have a fairly good understanding of the unpolarized component of the emission from our Milky Way and from distant galaxies (usually referred to as point sources).

The situation with regard to polarization is far worse. Both synchrotron and dust emission are expected to be polarized. In the case of synchrotron the theoretical maximum is 70%. Most of our knowledge about synchrotron polarization comes from surveys at relatively low frequencies. Extrapolation to frequencies where CMB experiments operate is severely hampered by Faraday rotation. Moreover, most modern surveys have concentrated on regions near the Galactic plane. How to extrapolate to higher latitudes remains unclear.

We will not dwell on foregrounds much longer because at this point there is not that much we can say. Time will tell if we are lucky again, as with the temperature anisotropies, or if foregrounds will spoil the potential fun of studying polarization. The interested reader is referred to the articles in the volume edited by de Oliveira-Costa & Tegmark (1999). More recent analysis of existing maps, some of which deal with the issue of whether foregrounds contaminate equally the E and B components can be found in a number of recent studies (Tucci et al. 2000, 2002; Baccigalupi et al. 2001; Bruscoli et al. 2002; Burigana & La

Porta 2002; Giardino et al. 2002). A recent summary including constraints coming from the PIQUE experiment is presented in de Oliveira-Costa et al. (2004). In the case of the DASI detection, the spectral index of the temperature anisotropies was very tightly constrained (ruling out any significant contamination there), and the temperature and polarization maps were correlated. This, together with the (rather weak) spectral index constraints from the polarization data, argued against any significant foreground contamination (Kovac et al. 2002).

1.5.4 $E-B$ Mixing: Systematic Effects

There are a variety of systematic effects that lead to mixing between E and B modes. In finite patches of sky, the separation cannot be done perfectly (Lewis, Challinor, & Turok 2002; Bunn et al. 2003). This is analogous to trying to decompose a vector field into its gradient and curl parts when it is measured on a finite part of a plane. Vector fields that are gradients of a scalar with zero Laplacian will have both zero curl and divergence. In fact, in a finite patch one can construct a basis for the polarization field in which basis vectors can be split into three categories. There are pure E, pure B, and a third category of modes that is ambiguous, which receives contributions from both E and B. The number of ambiguous modes is proportional the number of pixels along the boundary.

Aliasing due to pixelization mixes E and B; the power that is aliased from sub-pixel scales leaks into both E and B. This is particularly important because E polarization is expected to be much larger than B modes, and because the E polarization power spectra is relatively very blue.

Finally, other effects such as common mode and differential gain fluctuations, line cross-coupling, pointing errors, and differential polarized beam effects will create a spurious B signal from temperature and/or E components (Hu, Hedman, & Zaldarriaga 2003).

1.6 Conclusions

We have summarized the physics behind the generation of a small degree of polarization in the CMB. Quadrupole anisotropies in the radiation intensity at the last-scattering surface through Thomson scattering lead to a small degree of linear polarization. These quadrupole anisotropies can be generated by both density perturbations (mainly through "free streaming" of the Doppler effect) and by GW.

The quadrupole generated by GW leads to a distinct pattern of polarization on the sky. Such a pattern has a curl component, and thus the CMB polarization can serve as an indirect GW detector. If inflation is the source of the density perturbations, it is also expected to generate a stochastic background of GW. Searching for this background through CMB polarization has become one of the driving forces for the field. The level of the B component produced by GW is expected to be quite small, so the first generation of polarization experiments should see B modes consistent with zero.

After recombination several processes can affect polarization. Gravitational lensing distorts the polarization patter generating a B component, even in the absence of GW. This source of noise could become the final limit to the detectability of the GW background.

The reionization of the Universe provides a new opportunity for the CMB photons to scatter. It leaves a signature in the large-scale polarization, a bump in the power spectrum. If detected, it would help constrain the epoch of reionization and break many of the degeneracies that occur in CMB fits of cosmological parameters.

The DASI experiment has recently detected polarization. It found a pattern of polarization consistent with having no B modes, just as expected. It also favors a spectrum that rises toward small scales, just as the theory predicts. Moreover, it provides a tentative detection of a cross correlation between temperature and polarization at the level predicted by the model. The *WMAP* satellite already released a high signal-to-noise ratio measurement of the cross correlation between temperature and polarization. These results lead to the conclusion that the Universe reionized at a surprisingly high redshift and provided further evidence in favor of inflation. Everything is looking good. Time will tell if more sensitive polarization experiments will eventually fulfill their promise and help us solve some of the remaining mysteries about our Universe.

References

Baccigalupi, C., Burigana, C., Perrotta, F., De Zotti, G., La Porta, L., Maino, D., Maris, M., & Paladini, R. 2001 A&A, 372, 8
Benabed, K., Bernardeau, F., & van Waerbeke, L. 2001, Phys. Rev. D, 63, 43501
Bennett, C. L., et al. 2003, ApJS, 148, 1
Bernardeau, F. 1997, A&A, 324, 15
——. 1998, A&A, 338, 767
Bruscoli, M., Tucci, M., Natale, V., Carretti, E., Fabbri, R., Sbarra, C., & Cortiglioni, S. 2002, NewA, 7, 171
Bucher, M., Moodley, K., & Turok, N. 2000, Phys. Rev. D, 62, 083508
——. 2001, Phys. Rev. Lett., 87, 191301
Bunn, E. F., Zaldarriaga, M., Tegmark, M., & de Oliveira-Costa, A. 2003, Phys. Rev. D, 67, 023501
Burigana, C., & La Porta, L. 2002, in Astrophysical Polarized Backgrounds, ed. S. Cecchini et al. (Melville, NY: AIP), 54
Challinor, A., & Lasenby, A. 1999, ApJ, 513, 1
Coulson, D., Crittenden, R. G., & Turok, N. G. 1994, Phys. Rev. Lett., 73, 2390
Cooray, A., & Hu, W. 2001, ApJ, 548, 7
Crittenden, R. G., Coulson, D., & Turok, N. G. 1995, Phys. Rev. D, 52, 5402
Crittenden, R., Davis, R. L., & Steinhardt, P. J. 1993, ApJ, 417, L13
de Oliveira-Costa, A. & Tegmark, M., ed., 1999, Microwave Foregrounds (San Francisco: ASP)
de Oliveira-Costa, A., Tegmark, M., Zaldarriaga, M., Barkats, D., Gundersen, J. O., Hedman, M. M., Staggs, S. T., & Winstein, B. 2003, Phys. Rev. D, 67, 023003
de Oliveira-Costa, A., Tegmark, M., O'Dell, C., Keating, B., Timbie, P., Efstathiou, G., & Smoot, G. 2004, Phys. Rev. D, submitted (astro-ph/0212419)
Dodelson, S., Kinney, W. H., & Kolb, E. W. 1997, Phys. Rev. D, 56, 3207
Eisenstein, D. J., Hu, W., & Tegmark, M. 1999, ApJ518, 2
Fan, X., et al. 2002, AJ, 123, 1247
Giardino, G., Banday, A. J., Górski, K. M., Bennett, K., Jonas, J. L., & Tauber, J. 2002, A&A, 387, 82
Goldberg, D. M., & Spergel, D. N. 1999, Phys. Rev. D, 59, 103002
Hannestad, S., & Scherrer, R. J. 2001, Phys. Rev. D, 63, 083001
Hedman, M. M., Barkats, D., Gundersen, J. O., McMahon, J. J., Staggs, S. T., & Winstein, B. 2002, ApJ, 573, L73
Hinshaw, G., et al. 2003, ApJS, 148, 135
Hu, W. 2000, Phys. Rev. D, 62, 43007
——. 2001a, Phys. Rev. D, 64, 83005
——. 2001b, ApJ, 557, L79
——. 2003, Annals Phys., 303, 203
Hu, W., & Dodelson, S. 2002, ARA&A, 40, 171
Hu, W., Hedman, M. M., & Zaldarriaga, M. 2003, Phys. Rev. D, 67, 043004
Hu, W., & Holder, G. P. 2003, Phys. Rev. D, 68, 023001
Hu, W., & Okamoto, T. 2002, ApJ, 574, 566
Hu, W., Seljak, U., White, M., & Zaldarriaga, M. 1998, Phys. Rev. D, 57, 3290
Hu, W., Spergel, D. N., & White, M. 1997, Phys. Rev. D, 55, 3288
Hu, W., & Sugiyama, N. 1995, Phys. Rev D, 51, 2599
Hu, W., & White, M. 1996, Phys. Rev. Lett., 77, 1687
——. 1997, NewA, 2, 323

Kamionkowski, M., & Kosowsky, A. 1999, Annu. Rev. Nucl. Part. Sci., 49, 77
Kamionkowski, M., Kosowsky, A., & Stebbins, A. 1997a, Phys. Rev. Lett., 78, 2058
——. 1997b, Phys. Rev. D, 55, 7368
Kaplinghat, M., Chu, M., Haiman, Z., Holder, G., Knox, L., & Skordis, C. 2003a, ApJ, 583, 24
Kaplinghat, M., Knox, L., & Song, Y.-S. 2003b, astro-ph/0303344
Kaplinghat, M., Scherrer, R. J., & Turner, M. S. 1999, Phys. Rev. D, 60, 023516
Keating, B. G., O'Dell, C. W., de Oliveira-Costa, A., Klawikowski, S., Stebor, N., Piccirillo, L., Tegmark, M., & Timbie, P. T. 2001, ApJ560, L1
Kesden, M., Cooray, A., & Kamionkowski, M. 2002, Phys. Rev. Lett., 89, 11304
Kinney, W. H. 1998, Phys. Rev. D, 58, 123506
Knox, L., & Song, Y.-S. 2002, Phys. Rev. Lett., 89, 11303
Kogut, A., et al. 2003, ApJS, 148, 161
Kovac, J. M., Leitch, E. M., Pryke, C., Carlstrom, J. E., Halverson, N. W., & Holzapfel, W. L. 2002, Nature, 420, 772
Kosowsky, A. 1999, NewAR, 43, 157
Landau, S. J., Harari, D. D., & Zaldarriaga, M. 2001, Phys. Rev. D, 63, 83505
Leitch, E. M., et al. 2002, Nature, 420, 763
Lewis, A., Challinor, A., & Turok, N. 2002, Phys. Rev. D, 65, 23505
Lue, A., Wang, L., & Kamionkowski, M. 1999, Phys. Rev. Lett., 83, 1506
Ma, C.-P., & Bertschinger, E. 1995, ApJ, 455, 7
Mather, J. C., et al. 1994, ApJ, 420, 439
Mukhanov, V. 2003, astro-ph/0303072
Newman, E., & Penrose, R. 1966, J. Math. Phys., 7, 863
Okamoto, T., & Hu, W. 2002, Phys. Rev. D, 66, 63008
Ostriker, J. P., & Vishniac, E. T. 1986, ApJ, 306, L51
Peebles, P. J. E., Seager, S., & Hu, W. 2000, ApJ, 539, L1
Pen, U.-L., Seljak, U., & Turok, N. 1997, Phys. Rev. Lett., 79, 1611
Penzias, A. A., & Wilson, R. W. 1965, ApJ, 142, 419
Pieris, H. V., et al. 2003, ApJS, 148, 213
Polnarev, A. G. 1985, Soviet Astron., 62, 1041
Rebhan, A. K., & Schwarz, D. J. 1994, Phys. Rev. D, 50, 2541
Rees, M. J. 1968, ApJ, 153, L1
Sachs, R. K., & Wolfe, A. M. 1967, ApJ, 147, 73
Seager, S., Sasselov, D. D., & Scott, D. 1999, ApJ, 523, L1
Seljak, U. 1994, ApJ, 435, L87
——. 1996, ApJ, 482, 6
Seljak U., & Zaldarriaga M. 1996, ApJ, 469, 7
——. 1997, Phys. Rev. Lett., 78, 2054
——. 1999a, Phys. Rev. Lett., 82, 2636
——. 1999b, Phys. Rev. D, 60, 43504
——. 2000, ApJ, 538, 57
Silk, J. 1968, ApJ, 151, 459
Smoot, G. F., et al. 1992, ApJ, 369, L1
Song, Y.-S., Cooray, A., Knox, L., & Zaldarriaga, M. 2003, ApJ, 590, 664
Spergel, D. N., et al. 2003, ApJS, 148, 175
Spergel, D. N., & Goldberg, D. M. 1999, Phys. Rev. D, 59, 103001
Spergel, D. N., & Zaldarriaga, M. 1997, Phys. Rev. Lett., 79, 2180
Sunyaev, R. A., & Zel'dovich, Y. B. 1972, CommAp, 4, 173
Tegmark, M., & de Oliveira-Costa, A. 2001, Phys. Rev. D, 64, 63001
Tegmark, M., & Zaldarriaga, M. 2002, Phys. Rev. D, 66, 103508
Tucci, M., Carretti, E., Cecchini, S., Fabbri, R., Orsini, M., & Pierpaoli, E. 2000, NewA, 5, 181
Tucci, M., Carretti, E., Cecchini, S., Nicastro, L., Fabbri, R., Gaensler, B. M., Dickey, J. M., & McClure-Griffiths, N. M. 2002, ApJ, 579, 607
Turok, N. 1996a, Phys. Rev. Lett., 77, 4138
——. 1996b, Phys. Rev. D, 54,3686
Uzan, J.-P. 2003, Rev. Mod. Phys., 75, 403
Van Waerbeke, L., Bernardeau, F., & Benabed, K. 2000, ApJ, 540, 14

Weinberg, S. 2001a, Phys. Rev. D, 64, 123511
——. 2001b, Phys. Rev. D, 64, 123512
Wyithe, S., & Loeb, A. 2003, ApJ, 586, 693
Zahn, O., & Zaldarriaga, M. 2003, Phys. Rev. D, 67, 063002
Zaldarriaga, M. 1997, Phys. Rev. D, 55, 1822
——. 1998, ApJ, 503, 1
——. 2000, Phys. Rev. D, 62, 63510
Zaldarriaga, M., & Harari, D. 1995, Phys. Rev. D, 52, 3276
Zaldarriaga, M., & Seljak, U. 1997, Phys. Rev. D, 55, 1830
——. 1998, Phys. Rev. D, 58, 23003
——. 1999, Phys. Rev. D, 59, 123507
Zaldarriaga, M., Spergel, D. N., & Seljak, U. 1997, ApJ, 488, 1